Available online at www.sciencedirect.com
ScienceDirect
Trans. Nonferrous Met. Soc. China 24(2014) 1610−1618
Transactions of Nonferrous Metals Society of China
www.tnmsc.cn

Corrosion behavior of Hastelloy C22 coating produced by laser cladding in static and cavitation acid solution

Qin-ying WANG[1], Shu-lin BAI[1], Zong-de LIU[2]

1. HEDPS, Center for Applied Physics and Technology, LTCS, Department of Materials Science and Engineering, College of Engineering, Peking University, Beijing 100871, China;
2. Key Laboratory of Condition Monitoring and Control for Power Plant Equipment of Ministry of Education, North China Electric Power University, Beijing 102206, China

Received 14 June 2013; accepted 3 October 2013

Abstract: The Hastelloy C22 coatings on Q235 steel substrate were produced by high power diode laser cladding technique. Their corrosion behaviors in static and cavitation hydrochloric, sulfuric and nitric acid solutions were investigated. The electrochemical results show that corrosion resistance of coatings in static acid solutions is higher than that in cavitation ones. In each case, coating corrosion resistance in descending order is in nitric, sulfuric and hydrochloric acid solutions. Obvious erosion−corrosion morphology and serious intercrystalline corrosion of coating are noticed in cavitation hydrochloric acid solution. This is mainly ascribed to the aggressive ions in hydrochloric acid solution and mechanical effect from cavitation bubbles collapse. While coating after corrosion test in cavitation nitric acid solution shows nearly unchanged surface morphology. The results indicate that the associated action of cavitation and property of acid solution determines the corrosion development of coating. Hastelloy C22 coating exhibits better corrosion resistance in oxidizing acid solution for the stable formation of dense oxide film on the surface.
Key words: Hastelloy C22 coating; laser cladding; acid solution; cavitation corrosion; electrochemical impedance spectroscopy

1 Introduction

Hastelloy C22 exhibits more excellent anticorrosion property than most NiCrMo alloys, e.g. Hastelloy C276, C-4, Inconel 625, to pitting, crevice and stress corrosion. It is widely used in the chemical industry for the perfect corrosion resistance to chlorine, hot pollution solution, strong acid and alkali, organic solvents [1,2]. However, high cost of Hastelloy C22 sheet limits its large-scale applications. In recent decade, Hastelloy coatings have been rapidly developed by techniques of vacuum arc melting, casting, plasma spraying and laser cladding [3−5]. Among these, laser cladding is widely used to produce metallurgically well-bonded coating due to the advantages of high power, small heat-affected-zone (HAZ) and minimal distortion of the substrate [6−9]. HAEMERS et al [10] produced Hastelloy-C276 coating with a thickness of 3 mm by laser cladding technique. VIGNOLO et al [11] reported a synthesis of Hastelloy thin film by XeCl pulsed laser ablation. Then ZOCCO et al [3] found that the corrosion behavior of Hastelloy coating by XeCl pulsed laser ablation approximated to the bulk one. Thus, the previous researches have provided necessary methods to prepare Hastelloy C22 coating.

Various corrosion environments have been created to investigate the corrosion behavior of Hastelloy sheet. BELLANGER and RAMEAU [12] and TAKEUCHI et al [13] reported the corrosion behavior of Hastelloy C22 steel and C-276 in strong acid solution, respectively. HODGES et al [14] did research on the possibility of pit nucleation on Hastelloy C22 plate in LiCl solution. The electrochemical impedance spectroscopy of Hastelloy G-30 in continuous flowing seawater was obtained by Al-MUHANNA and HABIB [15]. ZOCCO et al [3] and VIGNOLO et al [11] mainly obtained corrosion behavior of corresponding Hastelloy coating in mixture solution of various salts with CO_2. In addition, cavitation damage including shock wave and micro-jet to the material surface owing to the repeated nucleation, growth and violent collapse of bubbles in the liquid, was also widely found in the chemical industry [16,17], e.g. the impeller of chemical pump. Cavitation can enhance

Corresponding author: Shu-lin BAI; Tel: +86-10-62759379; Fax: +86-10-62751812; E-mail: slbai@pku.edu.cn
DOI: 10.1016/S1003-6326(14)63232-5

electrochemical reaction and produce far more damage than static environment [18]. However, the corrosion behaviors of Hastelloy C22 coating on Q235 steel produced by high power diode laser cladding technique in various static and cavitation acid solutions were seldom investigated.

This work investigated the effects of cavitation and acid solution type on corrosion behavior of Hastelloy C22 coating prepared by high power diode laser cladding technique. The coatings were corroded in static and cavitation hydrochloric, sulfuric and nitric acid solutions, and the corresponding corrosion mechanisms were revealed in detail.

2 Experimental

2.1 Materials and laser cladding process

The chemical compositions of Hastelloy C22 powders and Q235 steel substrate are listed in Table 1. The preparation parameters of coating can be found in recent publication [19]. In this study, the coating by laser scanning speed of 6 mm/s was used. The as-prepared coating/substrate bulk was cut into dimensions of 10 mm×10 mm×4 mm. The top surface of samples were grinded with 2000 mesh abrasive papers and then polished with corundum powders of 3−5 μm, finally ultrasonically cleaned in distilled water followed by ethanol and acetone. The samples for electrochemical corrosion tests were covered with silica gel except an exposure a coating area of 10 mm×10 mm.

Table 1 Chemical compositions of Hastelloy C22 powders and Q235 steel

Sample	Mass fraction/%									
	Cr	Mo	Fe	W	Ni	Si	Mn	S	P	C
Powders	21.00	13.00	5.00	5.00	Bal.					
Q235 steel			Bal.			0.37	0.8	0.04	0.04	0.16

2.2 Methods

The hydrochloric (HA), sulfuric (SA) and nitric (NA) acid solutions with molar concentrations of 2 mol/L, 1 mol/L and 2 mol/L, respectively, were used in the corrosion tests, in which the same hydrogen ion concentration of 2 mol/L was kept. Electrochemical measurements in acid solutions with (called cavitation solution) and without (called static solution) ultrasonic excitation were carried out on an electrochemical workstation (CHI760, China) at 25 °C. Each test was repeated at least three times to obtain reliable results. The open circuit potential (OCP) was tested for 2 h in both conditions. The electrochemical impedance spectroscopy (EIS) in the static solution was measured every 30 min for 1.5 h in the frequency range from 100 kHz to 10 mHz, and voltage amplitude of ±5 mV. Then the potentiodynamic polarization curves were measured at the scanning speed of 1 mV/s from −0.5 to 1.5 V. The conventional three-electrode cell was used, with an Ag/AgCl/saturated KCl electrode as the reference electrode, a platinum electrode as the counter electrode and the coating sample as the working electrode.

The cavitation environment was created by an ultrasonic cleaner with an ultrasonic generator of frequency 40 kHz and output power of 100 W. The corrosion morphology of coating surface was observed by scanning electron microscopy (SEM, S-4800 HITACHI).

3 Results

3.1 Electrochemical corrosion measurements

3.1.1 Open circuit potential (OCP)

The variation of OCP with time for coatings in static and cavitation acid solutions is shown in Fig. 1. The smooth and unstable OCP curves are remarked in static and cavitation acid solutions, respectively. In the former case, OCP of coatings changes from positive to negative in the order of NA, SA and HA solutions. In static HA solution, the OCP decreases slowly as immersing time lasts. While in static SA solution, it increases at the beginning, and then decreases a little after 5 min until the end. Unlike two cases above, the continuously increasing OCP is found in static NA solution. However, the OCP exhibits different variation tendency with time in cavitation solution. In cavitation SA and NA solutions, the OCP is a little higher than that in static cases at the beginning, then is similar and lower at the end, respectively. As for cavitation HA solution, the OCP of coating keeps decreasing in the case in static solution but with lower value. In addition, the OCP curve in cavitation NA solution shows a drift at the potential of about 0.76 V.

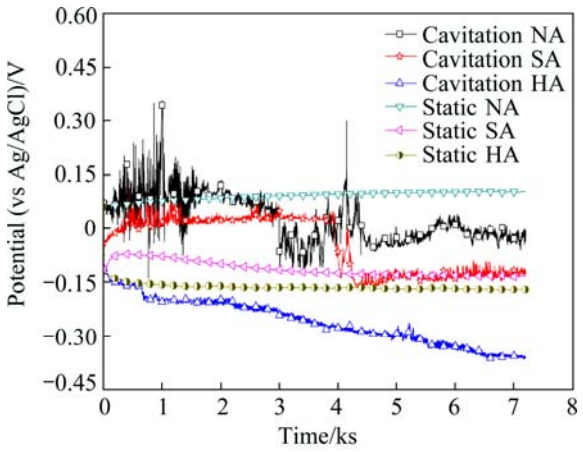

Fig. 1 OCP vs time of coatings in static and cavitation acid solutions

3.1.2 Polarization curves

The polarization curves of coatings tested at stable open circuit potential in static and cavitation acid solutions are shown in Fig. 2. In static solutions, both active and passive regions are noticed in the anodic polarization curve of coating in HA solution. Firstly, the corrosion current is enhanced by the increasing electrode potential. Then as the electrode potential reaches the passive potential of around −0.06 V, the corrosion current declines in the passive region from 0.2 to 0.9 V. As the electrode potential continues to increase, the transpassivation region is found and the corrosion current is improved dramatically. Unlike the case in HA solution, the polarization curves in the other two static solutions display the stable passive state as electrode potentials increase, and exhibit lower passive current density.

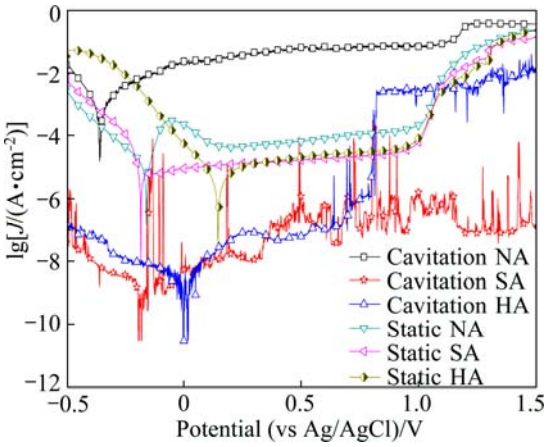

Fig. 2 Polarization curves of coatings in static and cavitation acid solutions

While the coatings in cavitation solutions show less positive corrosion potentials than those in static case. Meanwhile, the variation in corrosion current density is different in three acid solutions. The disappeared passive region and enhanced corrosion current density of coating are found in HA solution, but the lower corrosion current densities are observed in SA and NA solutions.

3.1.3 Electrochemical impedance spectroscopy (EIS)

The Nyquist plots of coatings in static solutions were obtained and demonstrated in Fig. 3, which reveal the electrochemical corrosion process. In Fig. 3(a), the nearly closed capacitive loop in the very beginning when the coating is immersed in HA solution shows the quick decline of impedance. Then the single capacitive loop develops into two loops at high and low frequency ranges, respectively, which is related with the electric double layer and broken oxide film on the coating surface. However, the completely different Nyquist plots are obtained in SA and NA solutions, as shown in Figs. 3 (b) and (c). In SA solution, the oxide film on the coating surface cannot be easily destroyed by sulfate radical,

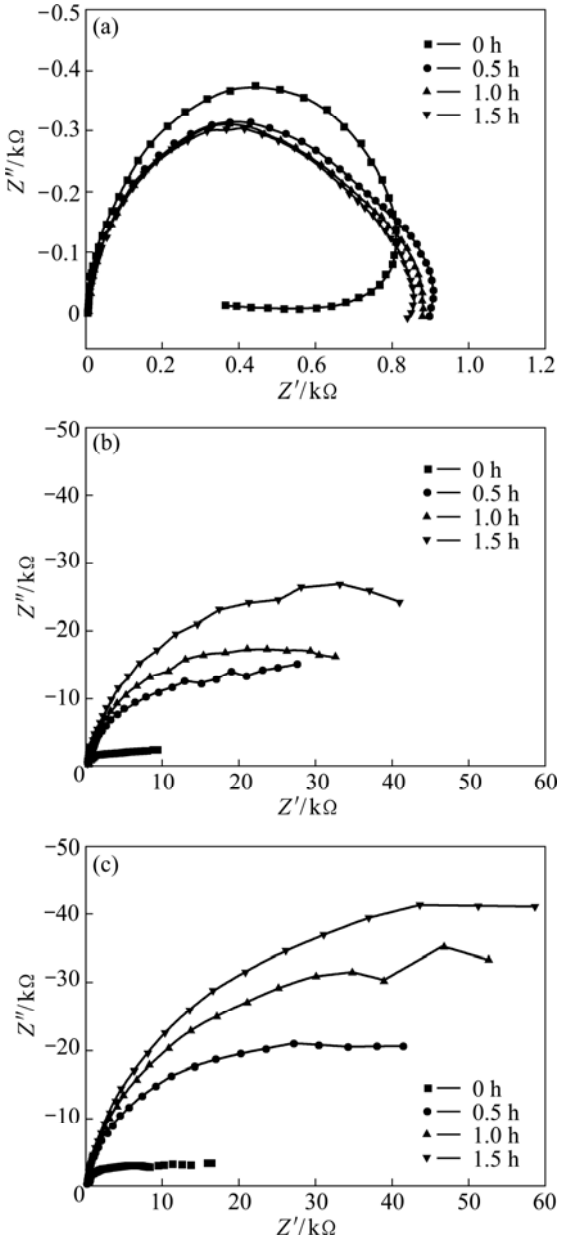

Fig. 3 Nyquist plots of coatings in static HA (a), SA (b) and NA (c) solutions

which limits the corrosion development to a certain degree. Therefore, the single capacitive loop expands gradually with time. While coating in NA solution shows larger radius of capacitive loop than that in SA solution, which reveals higher impedance and better surface state with oxide film. In addition, unfortunately, in the cavitation solutions, the coating surface state is so much disturbed by cavitation bubbles that smooth Nyquist plot curves cannot be obtained. However, according to the polarization curves in static and cavitation cases, it is reasonable to assume that the tendency of EIS results in cavitation solutions will be similar to those in static ones, but with lower radius of capacitive loops, meaning lower impedance.

3.2 Corrosion morphology

Surface morphologies of coatings before and after static corrosion tests in three acid solutions are shown in Figs. 4(a)−(d). The original coating surface is uniform and clean. For coating after corrosion test in HA solution, the clear microstructures of different regions signify the happening of apparent intergranular corrosion. While the coating surfaces are a little rough and white in SA and NA acid solutions, which is related with the oxidization of coating surface.

The surface morphologies in cavitation solution are shown in Figs. 4(e)−(g). In HA solution, the coating corrosion is enhanced by cavitation bubbles with shock wave and micro-jet. As for coatings in SA and NA solutions, the surface morphologies seem a little cleaner than those in static cases, which can be observed more clearly in Fig. 5. Meanwhile, a small quantity of erosion-corrosion sites are found on coating surface in SA solution, as marked with white circle, but without obvious intergranular corrosion.

The details of coating morphologies in static and cavitation solutions are shown in Fig. 5. The loosened corrosion products and slightly intercrystalline corrosion are observed on coating surface in static HA solution,

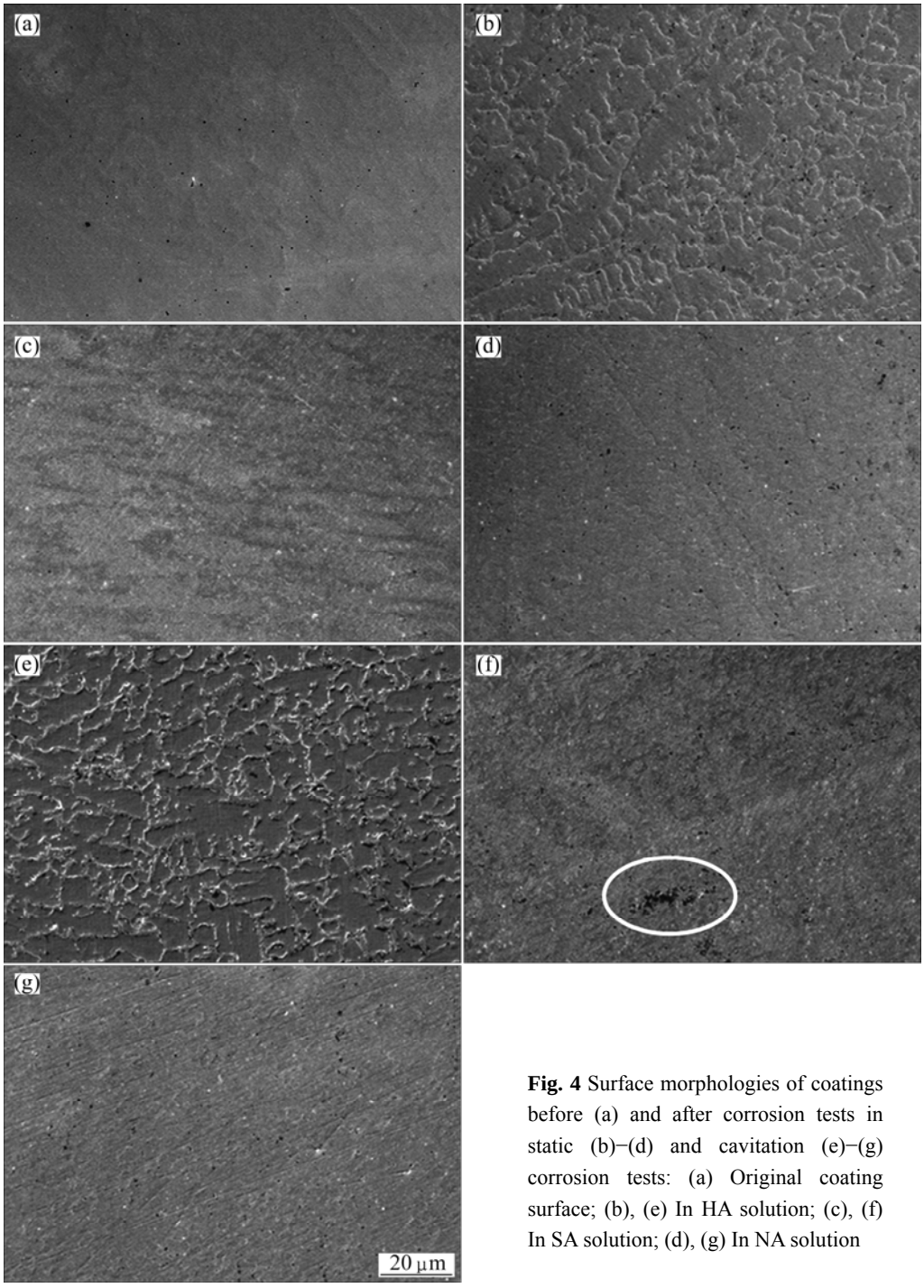

Fig. 4 Surface morphologies of coatings before (a) and after corrosion tests in static (b)−(d) and cavitation (e)−(g) corrosion tests: (a) Original coating surface; (b), (e) In HA solution; (c), (f) In SA solution; (d), (g) In NA solution

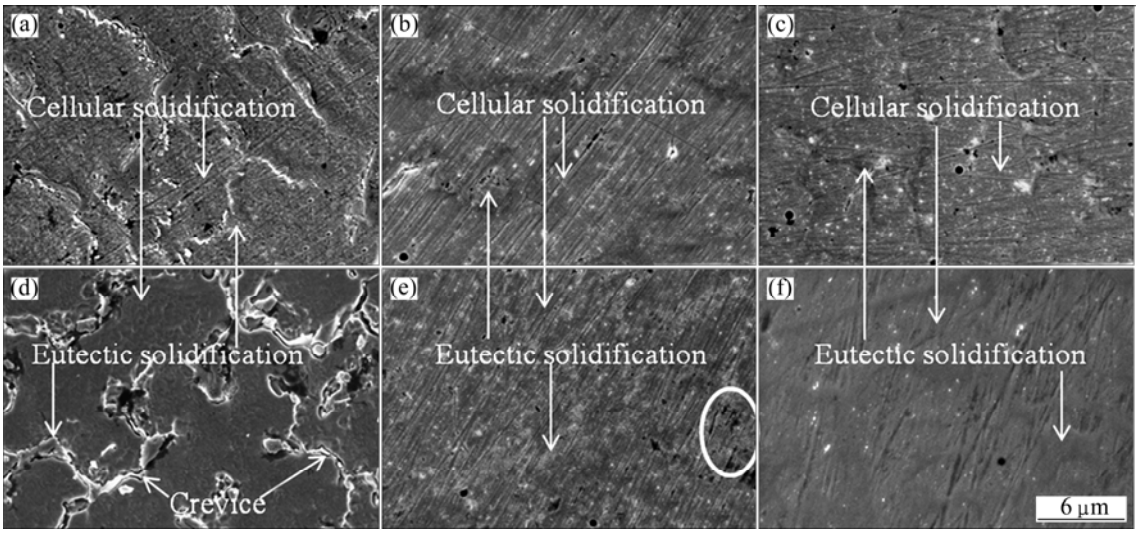

Fig. 5 Local morphologies after static ((a)−(c)) and cavitation ((d)−(f)) corrosion tests in three acid solutions: (a), (d) In HA solution; (b), (e) In SA solution; (c), (f) In NA solution

which reveals moderate corrosion of coating without erosion, as shown in Fig. 5(a). On the contrary, in corresponding cavitation case, the features of erosion−corrosion and intercrystalline corrosion are found, e.g. numerous shallow erosion sites at cellular solidification and crevices between cellular and eutectic solidifications, as shown in Fig. 5 (d). In addition, as mentioned above, coating surfaces in the other two cavitation solutions seem a little cleaner than those in static cases, but the erosion−corrosion sites can be observed in cavitation SA solution, revealing the damage of oxide film in some extent by cavitation bubbles collapse, as shown in Figs. 5(b) and (e). While, the similar damage on coating surface in cavitation NA solution is not found, which implies the minor effect of cavitation bubbles on coating corrosion (Figs. 5 (c) and (f)). The features of coating local morphologies in static and cavitation solutions are consistent with the electrochemical results in section 3.1.

4 Discussion

4.1 Effect of acid on corrosion resistance of coating

The OCP variation tendency of coatings from positive to negative in order of NA, SA and HA solutions can be explained according to the property of the acid, as shown in Fig. 1. Dilute HA and SA solutions used here display no oxidability, while dilute NA solution indeed exhibits oxidability. Thus coating in NA solution has a continuously increasing OCP curve with immersing time, which owes to continuously formed dense oxide film on the coating surface by oxidability. However, coatings show decreased OCP curve in HA solution and firstly increased and then decreased OCP curve in SA solution, to explain which, the anion must be considered. In HA solution, the chloride ion is a typical simple anion with smaller radius of 181 pm [20]. It can easily penetrate into the oxide film on the coating surface, and then destroy the oxide film and enhance the electrochemical reaction. While as for SA solution, two steps of corrosion should be taken into account: first, sulfate radical is a complicated anion with bigger radius, and thus cannot penetrate into the formed oxide film initially; second, when the immersing time reaches a critical value, the film is finally destroyed and the electrochemical reaction occurs inevitably. In addition, the stable OCP curves imply the tendency of thermodynamics. The more the positive OCP curve is, the more difficult the corrosion happening is, such as the coating in NA solution [21]. But in terms of corrosion rate after corrosion happens, the corrosion current density would be the determinant factor according to Faraday's law [22].

4.2 Effect of cavitation on corrosion resistance of coating

In cavitation solution, the bubbles collapse will act on coating in two ways. First, it promotes the formation of dense oxide film and shifts OCP by increasing mass transfer of oxygen [18,23]. Second, it can activate and destroy the oxide film to decrease OCP ascribed to high temperature and force from cavitation bubbles collapse. If the oxide film can form on coating surface in an acid solution without aggressive ions, the OCP curve will be determined by competition between above two ways,

namely for OCP curves in NA and SA solution, the first effect of cavitation is dominant in the beginning, but the second effect is dominant in turn after a period of time, as shown in Fig. 1. As for acid solution with aggressive ions, such as chloride ions in HA solution, the OCP will be aggravated mainly by the second effect without continuing to form oxide film. Furthermore, a drift at the potential about 0.76 V of the OCP curves in cavitation NA solution is found. This is also mainly ascribed to two aspects. First, the surface state of coating is unstable by cavitation with various effects, as mentioned above, leading to fluctuant OCP curves. Then, once the effect of "activateing and destroying the oxide film" by cavitation gets the upper hand at some time, the exposed fresh area will be under competition between forming and destroying oxide film from cavitation again, and the former is dominant with fresh area due to oxidation of NA solution. Thus it leads to the drift in the OCP curve of coating in cavitation NA solution.

In addition, the corrosion potential variations of coatings in static and cavitation solutions exhibit similar tendency, as shown in Fig. 2, but the lower cathodic and anodic current densities in cavitation NA and SA solutions than those in static cases are not consistent with some works [24, 25] that reported the enhanced current density by cavitation. In the process of the electrode reaction, the diffusion rate of corresponding ions to the coating surface is greatly accelerated by cavitation, thus diffusion process in the solution is not the rate-controlling step. As stated above, the oxide films exist on coating surface in NA and SA solutions, which would prevent harmful ions involved in the reaction from permeating into coating surface. This would be main rate-controlling step and result in lower cathodic and anodic current density in cavitation SA and NA solutions. On the contrary, for coating in cavitation HA solution, the electrode reaction is not limited by oxide film, thus has higher current density enhanced by cavitation.

4.3 Analysis of electrochemical impedance spectroscopy (EIS) in static solution

In consideration of the typical Nyquist plots, special corrosion morphologies of the coatings, as well as the properties of acid solutions [26], the equivalent circuits are proposed, as shown in Fig. 6, where R_s is solution resistance; R_{ox} and Q_{ox} are resistance and capacitance of the passive oxide film, respectively; R_{ct} is the charge transfer resistance; C_{dl} is the capacitance of the electric double layer; Z_w is the Warburg resistance.

The impedance expressions of equivalent circuits in Fig. 6 are expressed by [27]

$$Z_{H/S/N}=R_s+R_{ox}/[1+Y_0(j\omega)^nR_{ox}] \quad (1)$$

$$Z_H=R_s+(j\omega C_{dl}R_{ct}R_{ox}+R_{ct}+R_{ox})/[Y_0(j\omega)^n(j\omega C_{dl}R_{ct}R_{ox}+j\omega C_{dl}R_{ct}+R_{ct}+R_{ox}+1)] \quad (2)$$

$$Z_{S/N}=R_s+(R_{ox}+Z_w)/[1+Y_0(j\omega)^n(R_{ox}+Z_\omega)] \quad (3)$$

where $Z_{H/S/N}$ is the total impedance of coatings at the beginning of corrosion tests in three acid solutions; Z_H and $Z_{S/N}$ are the total impedance of coatings in HA solution and in the other two acid solutions after 30 min, respectively; ω is the frequency; Y_0 is the admittance; n is the dispersion coefficient.

In the beginning, coatings in three solutions have the same equivalent circuit shown in Fig. 6(a), which reveals the excellent protection of oxide film formed on the coating surface in the air with a high impedance resistance, a capacitance of low captance and a dispersion coefficient close to 1 [28]. As immersing time lasts, the different features of Nyquist plots are found between HA and the other two acid solutions, as shown

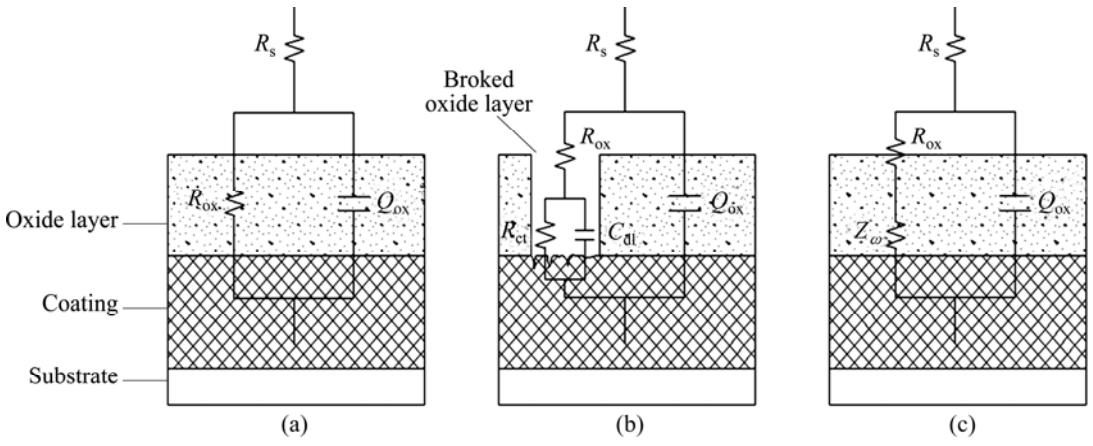

Fig. 6 Equivalent circuits of coatings at different conditions: (a) Beginning of corrosion tests; (b) In HA solution; (c) In SA or NA solution after 30 min

Table 2 Impedance parameters in HA, SA and NA solutions

Acid solution	Parameter	0	30 min	60 min	90 min
HA	R_s/(Ω·cm^2)	1.565	1.572	2.342	2.423
	R_{ox}/(Ω·cm^2)	756.9	718	0.8206	0.6449
	Y_0/(Ω^{-1}·cm^{-2}·s^n)	1.19×10^{-4}	1.7×10^{-4}	2.24×10^{-4}	2.12×10^{-4}
	n(0<n<1)	0.9092	0.8997	0.6546	0.7005
	C_{dl}/(F·cm^{-2})		4466	61.7	58.9
	R_{ct}/(Ω·cm^2)		184.2	882.4	850.9
SA	R_s/(Ω·cm^2)	2.771	2.326	2.677	2.587
	R_{ox}/(Ω·cm^2)	6987	2.23×10^4	3.33×10^4	4.78×10^4
	Y_0/(Ω^{-1}·cm^{-2}·s^n)	1.51×10^{-4}	1.03×10^{-4}	9.32×10^{-5}	9.37×10^{-5}
	n(0<n<1)	0.885	0.9197	0.9187	0.9164
	Z_o/(Ω·cm^2·s$^{-0.5}$)		2.69×10^{-4}	3.36×10^{-4}	2.25×10^{-4}
NA	R_s/(Ω·cm^2)	2.856	2.272	2.639	2.553
	R_{ox}/(Ω· cm^2)	1.18×10^4	4.00×10^4	5.74×10^4	7.13×10^4
	Y_0/(Ω^{-1}·cm^{-2}·s^n)	1.13×10^{-4}	8.52×10^{-5}	8.01×10^{-5}	7.66×10^{-5}
	n(0<n<1)	0.9029	0.9259	0.9272	0.9284
	Z_o/(Ω·cm^2·s$^{-0.5}$)		3.00×10^{-4}	1.77×10^{-4}	1.44×10^{-4}

in Fig. 3. In the former case, the equivalent circuit in Fig. 6(b) is used. It means that chloride ions can reach coating surface to produce corrosion and further intercrystalline crevices. Here, the electric double layer should be considered between oxide film and coating surface. In Table 2, corresponding parameter R_{ox} decreases with immersing time in HA solution, which means the increased damage of passive oxide film. While the variations of C_{dl} and R_{ct} are related with absorbed corrosion products. In the case of SA and NA solutions, the same equivalent circuit is shown in Fig. 6(c). It can be seen that the denser oxide film plays a key role in the coating corrosion resistance. The corrosion process turns to be controlled by the film resistance and thickness of diffusion layer. The increased R_{ox} in SA and NA solutions in Table 2 indicate more densely protective oxide films on the coating surfaces. Meanwhile, coating in NA solution has better corrosion resistance than that in SA solution. The decreased Z_w in these two acid solutions implies the decreased diffusion layer [29], which is beneficial to reduce the corrosion because the diffusion of ions involved in the electrochemical reaction is minimized to the coating surface.

4.4 Corrosion morphology analysis

The corrosion morphologies of coatings clearly reflect the effects of acid solution and cavitation. Aggressive chloride ions in HA solution can penetrate into the oxide film to destroy preferentially the regions between primary and eutectic solidifications, and finally form soluble chloride to aggravate oxide film degradation [30]. This process is aggravated by cavitation with clearer crevices and erosion morphology by removing the corrosion products and revealing the fresh area to enhance the electrochemical reaction. In addition, coating in cavitation SA solution shows a small quantity of erosion−corrosion sites rather than in static case, revealing the damage of cavitation. However, the damage is not found on coating surfaces in both static and cavitation NA solutions, showing the protection of oxide film and also implying the important role of acid oxidation in both solutions.

5 Conclusions

1) The cavitation corrosion is more serious than static corrosion, which is manifested by the less positive corrosion potentials. This remarkable difference is ascribed to the combined mechanical and electrochemical effects on the corrosion behavior from the collapse of numerous cavitation bubbles. However, if the acid solution doesn't contain aggressive ions, such as nitric and sulfuric acid solutions, the impact of bubble collapse is not as strong as to completely destroy the oxide film, thus the cavitation effect is much reduced.

2) The chloride ions in hydrochloric acid solution are so aggressive that they can penetrate into the oxide film and result in serious corrosion. In this case, the corrosion process is also aggravated by the cavitation. Therefore, the associated action of cavitation and

aggressive ions promotes the corrosion development. Overall, Hastelloy C22 coating is more resistant to corrosion in oxidizing acid solution for the stable formation of dense oxide film on the surface.

References

[1] CROOK P. Corrosion characteristics of the wrought Ni−Cr−Mo alloys [J]. Materials and Corrosion, 2005, 56(9): 606−610.

[2] REBAK R B, CROOK P. Influence of the environment on the general corrosion rate of alloy 22 (N06022) [C]//ASME/JSME 2004 Pressure Vessels and Piping Conference. San Diego: American Society of Mechanical Engineers, 2004: 131−136.

[3] ZOCCO A, PERRONE A, VIGNOLO M F, DUHALDE S, AVRAM I, MORALES C, PEREZ T. High quality Hastelloy films deposited by XeCl pulsed laser ablation [J]. Applied Surface Science, 2003, 208−209: 669−675.

[4] KURODA S, FUKUSHIMA T, SASAKI M, KODAMA T. Microstructure and corrosion resistance of HVOF sprayed 316L stainless steel and Hastelloy C coatings [J]. Materials Transactions, 2002, 43(12): 3177−3183.

[5] NIRANATLUMPONG P, KOIPRASERT H. Improved corrosion resistance of thermally sprayed coating via surface grinding and electroplating techniques [J]. Surface and Coatings Technology, 2006, 201(3): 737−743.

[6] CUI C, GUO Z, LIU Y, XIE Q, WANG Z, HU J, YAO Y. Characteristics of cobalt-based alloy coating on tool steel prepared by powder feeding laser cladding [J]. Optics & Laser Technology, 2007, 39(8): 1544−1550.

[7] DEHM G, BAMBERGER M. Laser cladding of Co-based hardfacing on Cu substrate [J]. Journal of Materials Science, 2002, 37(24): 5345−5353.

[8] ZHOU S, DAI X, ZHENG H. Analytical modeling and experimental investigation of laser induction hybrid rapid cladding for Ni-based WC composite coatings [J]. Optics & Laser Technology, 2011, 43(3): 613−621.

[9] YELLUP J M. Laser cladding using the powder blowing technique [J]. Surface and Coatings Technology, 1995, 71(2): 121−128.

[10] HAEMERS T A M, RICKERBY D G, LANZA F, GEIGER F, MITTEMEIJER E J. Laser cladding of stainless steel with Hastelloy [J]. Advanced Engineering Materials, 2001, 3(4): 242−245.

[11] VIGNOLO M F, AVRAM I, DUHALDE S, MORALES C, PEREZ T, CULTRERA L, PERRONE A, ZOCCO A. Characterization of Hastelloy thin films deposited by pulsed laser ablation [J]. Applied Surface Science, 2002, 197−198: 343−347.

[12] BELLANGER G, RAMEAU J J. Behaviour of Hastelloy C22 steel in sulphate solutions at pH 3 and low temperatures [J]. Journal of Materials Science, 1996, 31(8): 2097−2108.

[13] TAKEUCHI M, NAKAJIMA Y, HOSHINO K, KAWAMURA F. Controls of chromium and third element contents in nickel-base alloys for corrosion resistant alloys in hot HNO_3–HF mixtures [J]. Journal of Alloys and Compounds, 2010, 506(1): 194−200.

[14] HODGES S, LAYCOCK N J, KROUSE D P, VIRTANEN S, SCHMUTZ P, RYAN M P. A microelectrochemical investigation of alloy C22 in chloride solutions below the critical pitting temperature [J]. Journal of the Electrochemical Society, 2007, 154(2): C114−C119.

[15] AL-MUHANNA K, HABIB K. Corrosion behavior of different alloys exposed to continuous flowing seawater by electrochemical impedance spectroscopy (EIS) [J]. Desalination, 2010, 250(1): 404−407.

[16] LIU C, LI J, CHEN H. Cavitation erosion on solid polymers of polytetrafluoroethelyene [J]. Tribology Letters, 2012, 47(1): 17−20.

[17] MANN B S, ARYA V, PANT B K. Cavitation erosion behavior of HPDL-treated TWAS-coated Ti6Al4V alloy and its similarity with water droplet erosion [J]. Journal of Materials Engineering and Performance, 2011, 21(6): 849−853.

[18] RYL J, DAROWICKI K, SLEPSKI P. Evaluation of cavitation erosion–corrosion degradation of mild steel by means of dynamic impedance spectroscopy in galvanostatic mode [J]. Corrosion Science, 2011, 53(5): 1873−1879.

[19] WANG Q Y, ZHANG Y F, BAI S L, LIU Z D. Microstructures, mechanical properties and corrosion resistance of Hastelloy C22 coating produced by laser cladding [J]. Journal of Alloys and Compounds, 2013, 553: 253−258.

[20] JIANG S L, ZHENG Y G, YAO Z M. Cavitation erosion behaviour of 20SiMn low alloy steel in Na_2SO_4 and $NaHCO_3$ solutions [J]. Corrosion Science, 2006, 48(9): 2614−2632.

[21] CAO C N. Principles of electrochemistry of corrosion [M]. Beijing: Chemical Industry Press, 2008. (in Chinese)

[22] QIAN M, LI D, LIU S B, GONG S L. Corrosion performance of laser-remelted Al−Si coating on magnesium alloy AZ91D [J]. Corrosion Science, 2010, 52(10): 3554−3560.

[23] GARCIA-GARCIA D M, GARCIA-ANTON J, IGUAL-MUNOZ A. BLASCO-TAMARIT E. Effect of cavitation on the corrosion behaviour of welded and non-welded duplex stainless steel in aqueous LiBr solutions [J]. Corrosion Science, 2006, 48(9): 2380−2405.

[24] GARCIA-GARCIA D M, BLASCO-TAMARIT E, GARCIA-ANTON J. Effects of the area of a duplex stainless steel exposed to corrosion on the cathodic and anodic reactions in a LiBr solution under static and dynamic conditions [J]. International Journal of Electrochemical Science, 2011, 6: 1237−1249.

[25] YU H, ZHENG Y G, YAO Z M. The cavitation erosion and erosion-corrosion behavior of carbon steel in simulating solutions of three rivers of China [J]. Materials and Corrosion, 2006, 57(9): 705−714.

[26] WANG R R. Acid structure and characteristic [M]. Hangzhou: Zhejiang Education Press, 1985. (in Chinese)

[27] CAO C N, ZHANG J Q. An introduction to electrochemical impedance spectroscopy [M]. Beijing: Science Press, 2002. (in Chinese)

[28] ZENG C L, WANG W, Wu W T. Electrochemical-impedance study of the corrosion of Ni and FeAl intermetallic alloy in molten (0.62Li, 0.38K)$_2CO_3$ at 650 °C [J]. Oxidation of Metals, 2000, 53(3−4): 289−302.

[29] DOKKO K, FUJITA Y, MOHAMEDI M, UMEDA M, UCHIDA I, SELMAN J R. Electrochemical impedance study of Li-ion insertion into mesocarbon microbead single particle electrode Part II. Disordered carbon [J]. Electrochimica Acta, 2001, 47(6): 933−938.

[30] SHALABY H M. Failure of Hastelloy C-276 pump impeller in hydrochloric acid [J]. Engineering Failure Analysis, 2008, 15(5): 543−546.

激光熔覆哈氏合金 C22 涂层在静态和空化酸溶液中的腐蚀行为

王勤英[1]，白树林[1]，刘宗德[2]

1. 北京大学 工学院，材料科学与工程系，高能量密度物理数值模拟教育部重点实验室，
应用物理与技术研究中心, 湍流与复杂系统国家重点实验室，北京 100871；
2. 华北电力大学 电站设备状态检测与控制教育部重点实验室，北京 102206

摘 要：利用高功率半导体激光器在 Q235 钢基体上制备哈氏合金 C22 涂层，研究涂层在静态和空化盐酸、硫酸和硝酸溶液中的腐蚀行为。电化学结果表明：涂层在静态酸溶液中比在空化酸溶液中具有更强的抗腐蚀性能。在以上的每种条件下，涂层抗腐蚀性能由强到弱的顺序均为硝酸、硫酸和盐酸溶液。涂层在空化盐酸溶液中出现冲蚀形貌和严重的晶间腐蚀。这主要与盐酸溶液中存在活性离子以及空化泡崩溃时的力学作用有关。然而，经过空化硝酸溶液腐蚀的涂层表面几乎没有变化。结果表明，空化作用和酸溶液性质的共同作用决定涂层腐蚀的发展。由于在表面形成稳定的致密氧化膜，哈氏合金 C22 涂层在氧化性酸溶液中表现出更优越的抗腐蚀性能。

关键词：哈氏合金 C22 涂层；激光熔覆；酸溶液；空化腐蚀；电化学阻抗

(Edited by Chao WANG)